

Doping helium nanodroplets with high temperature metals: Formation of chromium clusters

Martin Ratschek, Markus Koch, and Wolfgang E. Ernst

Citation: *J. Chem. Phys.* **136**, 104201 (2012); doi: 10.1063/1.3692330

View online: <http://dx.doi.org/10.1063/1.3692330>

View Table of Contents: <http://jcp.aip.org/resource/1/JCPSA6/v136/i10>

Published by the [American Institute of Physics](#).

Additional information on J. Chem. Phys.


Journal Homepage: <http://jcp.aip.org/>

Journal Information: http://jcp.aip.org/about/about_the_journal

Top downloads: http://jcp.aip.org/features/most_downloaded

Information for Authors: <http://jcp.aip.org/authors>

ADVERTISEMENT



AIPAdvances

Special Topic Section:
PHYSICS OF CANCER

Why cancer? Why physics? [View Articles Now](#)

Doping helium nanodroplets with high temperature metals: Formation of chromium clusters

Martin Ratschek, Markus Koch,^{a)} and Wolfgang E. Ernst

Institute of Experimental Physics, TU Graz, Petersgasse 16, A-8010 Graz, Austria

(Received 11 January 2012; accepted 18 February 2012; published online 13 March 2012)

A new method for stable and continuous doping of superfluid helium nanodroplets (He_N) with high-melting elements such as refractory metals is presented. The method exploits the advantages of electron bombardment heating and avoids stray fields induced by high currents or high frequency fields. It is thus especially suitable for magnetic studies of atoms and clusters in He_N . The source is characterized by means of mass spectroscopic investigations of He_N doped with chromium atoms and clusters. Source temperatures of up to $(1650 \pm 50)^\circ\text{C}$ were reached and Cr clusters up to Cr_9 could be formed in He_N . © 2012 American Institute of Physics. [<http://dx.doi.org/10.1063/1.3692330>]

I. INTRODUCTION

Knowledge about the electronic and magnetic properties of nanoclusters is essential as they are considered as building blocks of novel materials. The distribution of charges as well as orbital and spin angular momenta in clusters may be observed in electric and magnetic dipole moment measurements.¹ While isolated atoms of almost all elements show a non-vanishing magnetic moment (described by Hund's rule), in the solid state only very few elements preserve a magnetization. This is a consequence of electron delocalization, favoring equal population of states with antiparallel spin orientation. The understanding of property change in the transition from a high electron density in isolated atoms to a dilute electron gas in solids is thus one of the main goals in cluster theory.²

Chromium (Cr) is of high fundamental interest because of the large magnetic moment of single Cr atoms (6 Bohr magnetons), caused by their ground state electronic configuration ($[\text{Ar}] 3d^5 4s; ^7S_3$). The Cr dimer exhibits a metal-metal multiple bonding character. In contrast to its high number of six electron pairs that occupy the region between the two bonded atoms—the highest multiplicity that can be achieved between two equal atoms—the binding energy of (1.54 ± 0.06) eV (Ref. 3) is surprisingly low. This discrepancy is attributed to the differences in size between the $3d$ and $4s$ orbitals and is less pronounced in the heavier group 6 elements due to relativistic effects.⁴ Clusters of transition metals with nearly half filled shells, such as Cr and manganese (Mn), are of particular interest due to the large number of unpaired electrons per atom and the related possibility of huge local spin polarization. This is demonstrated in Stern–Gerlach deflection experiments of Cr_n ($n = 20$ –133), where superparamagnetic response is found and cluster magnetic moments per atom often far exceed the moment per atom present anywhere in the bulk antiferromagnetic lattice.⁵

In rare gas matrices (Ar, Kr, and Xe) Cr atoms,^{6,7} Cr_2 ,^{8,9} and Cr_3 molecules¹⁰ have been investigated. The transition from atomic properties to bulk properties was studied both experimentally^{5,11} and theoretically.^{12,13} Because of the magnetic properties of Cr, magnetic resonance techniques such as electron spin resonance (ESR) are particularly suitable for probing the electronic structure. Cr atoms and clusters were studied by means of ESR in Ne, Ar, and Kr matrices.¹⁴

Seeded beam and matrix isolation experiments, however, show some disadvantages. Metal clusters produced by seeded beams can usually be considered as hot with temperatures of 25 K and higher. In solid matrices, the perturbation by the host is strong and depends on the lattice site, while in liquid matrices a non-steady state dopant distribution is caused by diffusion. Also, in both solid and liquid matrices the localization of the dopants cannot be controlled on atomic scale. These problems can be overcome with helium nanodroplet isolation spectroscopy (HENDI), which is described in detail in Refs. 15 and 16. Helium nanodroplets (He_N) are transparent from the far IR to the vacuum UV. Almost any species brought into gas phase can be picked up and confined in the droplets. The dopants are immediately cooled to the droplet temperature of 0.37 K by evaporative cooling and are thus in the ground state. High versatility in doping, the possibility of successive particle pickup, and high dopant mobility due to the superfluidity of He_N allows tailoring of desired complexes, especially the formation of metal clusters.¹⁷ Recently, large silver (Ag) clusters have been formed in He_N and investigated by photoabsorption¹⁸ as well as transmission electron microscopy upon surface deposition.¹⁹ The low-temperature superfluid environment of a He_N affects the cluster formation process, especially regarding magnetic properties of the formed clusters. Alkali-metal oligomers are found in high-spin states on He_N (Refs. 20 and 21) since the formation of low-spin states will release enough energy to detach the molecules from the droplets. Silver dimers inside He_N form triplet states.²² This indicates also the possibility of the formation of a high-spin state of Cr clusters in He_N . In terms of characterization, ESR of single alkali-metal atoms on He_N has recently been achieved for the first time.²³ The absence

^{a)} Author to whom correspondence should be addressed. Electronic mail: markus.koch@tugraz.at.

of spin-relaxation mechanisms results in long spin lifetimes and coherent population transfer (Rabi oscillations) could be demonstrated. The weak perturbation by the He_N causes only minor line shifts in the hyperfine-resolved ESR spectra.²⁴ Additionally, magnetic dichroism studies give information about the magnetic properties of atoms and oligomers on He_N .^{25–27}

To dope He_N with single or multiple Cr atoms, the metal has to be brought into the gas phase. In spite of the relatively high vapor pressure compared to other metals with a similar melting point, elevated temperatures between 1300 °C and 1700 °C are required. While temperatures up to 800 °C can be easily achieved in resistively heated ovens,²⁸ higher temperatures require induction heating (e.g., 2500 °C and higher²⁹) or laser ablation.³⁰ Both techniques have, however, certain disadvantages in combination with the experimental needs of our ESR experiment. Resistive and induction heating cause magnetic stray fields, either due to the high currents used or due to the emitted radio frequencies, respectively. For example, a current of 100 A at our pickup region causes a stray field in the microwave cavity³¹ that is twice as high as the ESR linewidth.²³ Laser ablation, on the other hand, is a pulsed source with a non-steady-state distribution of the ablation signal.³⁰ For the preparation of a seeded beam of high temperature radicals, Steimle *et al.* used a cw electron bombardment source.³² The development of such an electron bombardment evaporation source (EBES) expands the variety of dopants to refractory materials which is the first step towards optical and magnetic resonance studies of high-melting elements and their clusters isolated in He_N . The continuous source and the low magnetic stray field are important requirements for such experiments. Also, our crossed beam configuration (see below) avoids surface deposition of single atoms effusing from the pickup source. We note that evaporation sources based on electron bombardment are commercially available but do not fulfil our requirements in terms of flux rate and metal ion formation.

As a first demonstration we dope He_N with Cr. We observe the formation of Cr clusters with up to 9 Cr atoms and characterize the pickup process with mass spectroscopic methods.

II. EXPERIMENTAL SECTION

A. Helium nanodroplet beam apparatus

The setup follows the typical design of a HENDI apparatus.¹⁵ Our machine including all measurement schemes is described in detail in Ref. 31. The apparatus is divided into four differentially pumped sections: the source-, pickup-, measurement-, and quadrupole mass spectrometer (QMS) chamber. In the source chamber, the He_N beam is formed by a supersonic expansion from a cooled nozzle (5 μm diameter, $p_0 = 40$ –80 bar stagnation pressure, and $T_0 = 10$ –30 K temperature). The resulting He_N size distribution is described by a log-normal function³³ and the distribution maximum \hat{N}_{p_0, T_0} can be calculated.^{34–36} Typical values, as used for the experiments presented here, are $\hat{N}_{50, 15} = 5900$ and $\hat{N}_{75, 14} = 8700$ (the corresponding mean droplet sizes are $\bar{N}_{50, 15} = 11\,500$ and $\bar{N}_{75, 14} = 21\,700$, respectively).

The He_N beam is collimated by a skimmer (300 μm diameter) and subsequently passes into the pickup chamber for doping. Usually, He_N are doped by passing through a pickup cell containing vapor of the desired species (typically 10^{-5} mbar in a ~ 3 cm long cell for single particle pickup). Here, the EBES forms an effusive atomic beam which crosses the He_N beam perpendicularly for doping (for construction details see Sec. II B). Multiple particle pickup can be achieved by increasing the flux rate and approximately follows a Poisson distribution.³⁷ The doped He_N can be studied in the third chamber. Between electromagnet pole shoes, two laser interaction zones and a photomultiplier allow optical spectroscopy including pump–probe experiments and magnetic circular dichroism studies on dopant atoms and molecules.^{25, 38} In combination with an ESR cavity in between the laser intersections optically detected magnetic resonance studies were carried out on potassium and rubidium.^{23, 24, 31, 39} We intend to apply these techniques to Cr doped He_N . In the last chamber, a QMS combined with electron impact ionization (Balzers PPM 422) is used to analyze dopant products.

B. Electron bombardment evaporation source

A schematic drawing and a photograph of the EBES are shown in Fig. 1. The oven is mounted on three stainless steel threaded rods (M4 size) which are kept in place by a fixation ring. A tantalum (Ta) crucible (16 mm outer diameter) is clamped between two ceramic tubes (aluminum oxide), which are placed in a notch of the crucible. The crucible is covered with a slit aperture (slit: 2 mm \times 10 mm) made of a Ta sheet. The ceramic tubes provide electrical and thermal insulation. Each tube is fixed between two conically shaped screws, which are connected to the threaded rods. Electrons are thermally emitted from two resistively heated tungsten

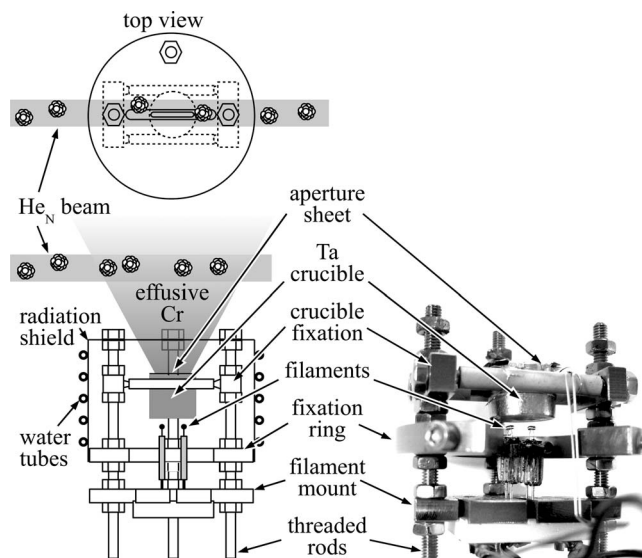


FIG. 1. Top and side view (left) and photograph (right) of the electron bombardment source: electrons are thermally emitted from two filaments mounted beneath the Ta crucible, which contains Cr metal. The electrons are accelerated in an electric field onto the crucible, thereby heating the Cr. The He_N beam is crossed by the evaporated Cr atoms perpendicularly to facilitate the pickup.

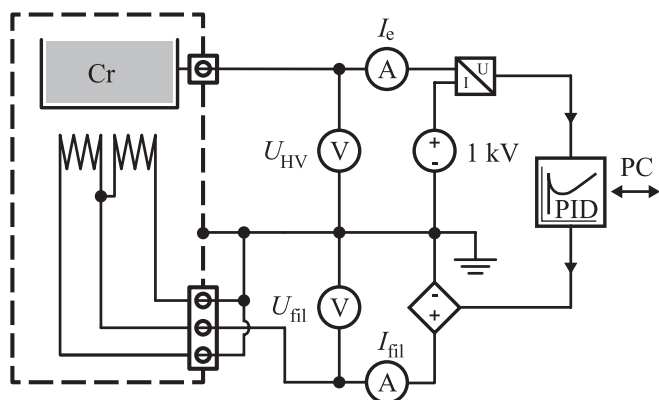


FIG. 2. Control circuit of the EBES: a PID controller provides constant heating power ($P_{\text{EBES}} \propto I_e$). The emission current I_e is stabilized by controlling the filament voltage U_{fil} . The high voltage U_{HV} is constant (1 kV) and the filament current I_{fil} can be monitored. The dashed line indicates the vacuum chamber. The PID controller is connected to a computer (PC) for data acquisition.

filaments beneath the crucible (standard 12 V halogen bulb lamps, nominal power 20 W, glass bulb removed) and accelerated to the crucible. The filaments are inserted into the filament mount (a combination of stainless steel and Macor[®]), which also provides electrical contacting. The distance between filaments and crucible (typically ~ 2 mm) is crucial for stable operation. Smaller distances increase the heating power but facilitate electrical breakdowns. The EBES is enclosed in a water cooled copper radiation shield, which is also equipped with a slit on the upper side. The slit aperture of the crucible and the slit of the radiation shield are both aligned parallel to the He_N beam. The distance between the crucible and the radiation shield has to be larger than ~ 10 mm for stable operation. This leads to a crucible to He_N beam distance of ~ 15 mm. It is also important that the pressure in the pickup chamber is at least in the 10^{-6} mbar regime.

The filaments are usually operated simultaneously and connected in parallel, as shown in Fig. 2. Emitted electrons are accelerated in an electric field at a fixed voltage of $U_{\text{HV}} = 1$ kV (power supply: Kaiser Systems Inc. Series 5000; max: 1 kV, 1 A) onto the Ta crucible. A proportional integral derivative (PID) controller (Eurotherm 3204) stabilizes the emission current I_e and thus the EBES heating power P_{EBES} by controlling the filament voltage U_{fil} . Typical values are $U_{\text{fil}} = 10$ V and $I_{\text{fil}} = 3$ A (standard dc power supply with analog input; max: 32 V, 10 A). With $I_e = 200$ mA, corresponding to $P_{\text{EBES}} = 200$ W, we reach EBES temperatures T_{EBES} of $(1650 \pm 50)^\circ\text{C}$. Stable conditions are established with maximum emission currents between 100 mA and 150 mA per filament. The temperature of the Ta crucible was measured with a two channel pyrometer (Raytek MRS1) through an acrylic glass window operating the EBES without the water cooled radiation shield. The pyrometer in combination with the acrylic glass window was calibrated with a black body radiation source.

At these elevated temperatures thermal radiation both from the Ta crucible and the filaments leads to increased background signals at optical detectors. Therefore, we use the EBES in an own vacuum chamber well separated from the

photomultiplier. Apertures and optical filters can be used to further reduce the stray light.

The maximum temperature of the source is in principle limited by alloying and reactions of the test species with the crucible material, which is typically happening between 2000°C to 2200°C depending on the materials. To reach higher temperatures than 1700°C further steps are to be taken: (1) An additional radiation shield around the crucible will reduce the radiation loss and thus increase the oven temperature for the same heating power. (2) An increase in the acceleration voltage will directly affect the heating power. Up to 10 kV can be used²⁹ but higher acceleration voltages will increase the X-ray emission. (3) The emission current, also directly proportional to the heating power, can be increased by raising the filament's temperature. (4) Reducing the work function of the filament's material will increase the emission current. The work function can be decreased by replacing the pure tungsten filaments with, for example, thorium or rhenium coated filaments. (5) Additional filaments will increase the area for electron emission and thus the emission current.

III. RESULTS AND DISCUSSION

We show the first doping of He_N with Cr atoms and the formation of Cr clusters in He_N up to Cr_9 . In these experiments, the He_N source parameters (stagnation pressure p_0 and nozzle temperature T_0) and the EBES heating power P_{EBES} are optimized for few and multi-Cr atom pickup, respectively. For the pickup of few Cr atoms, we use a high flux rate of relatively small He_N . With $p_0 = 50$ bar and $T_0 = 15$ K we obtain a droplet size distribution maximum of $\dot{N}_{50,15} = 5900$ atoms per droplet.^{34–36} These source conditions are used for the measurement of pickup statistics (Fig. 3), where P_{EBES} is increased continuously, and for the measurement of a Cr_n ($1 \leq n \leq 6$) mass spectrum at $P_{\text{EBES}} = 160$ W (Fig. 4). To show the formation of larger Cr_n (n up to 9, Fig. 5), the He_N source parameters were changed to $p_0 = 75$ bar and $T_0 = 14$ K to optimize for a high flux of larger droplets with $\dot{N}_{75,14} = 8700$ atoms. The corresponding value of P_{EBES} was 180 W.

The pickup statistics shown in Fig. 3 illustrate the dependency of the QMS ion signal on P_{EBES} . We monitor the masses 8 u (He_2^+), 52 u (Cr^+), 104 u (Cr_2^+), and 260 u (Cr_5^+), while raising P_{EBES} continuously up to 225 W. The He_2^+ signal is used as indicator for the overall He_N beam intensity. The maxima of the Cr^+ , Cr_2^+ , and Cr_5^+ signals appear at increased heating powers, as expected. We note that electron impact ionization of the doped droplets may cause fragmentation of larger Cr oligomers. The Cr^+ monomer ion signal may thus be higher than the actual flux rate of He_N doped with single Cr atoms, especially in regions of P_{EBES} where multiple Cr pickup is favored. Nevertheless, the appearance of Cr_2^+ and Cr_5^+ signal maxima clearly demonstrates that a certain fraction of Cr oligomers is not fragmented.

The He_2^+ signal drops rapidly at $P_{\text{EBES}} > 150$ W. We allocate the appearance of He_2^+ signal at 8 u to the existence of bare, undoped He_N . The drop can thus be explained by the decreasing probability of He_N to remain undoped.⁴⁰ Also, smaller He_N may be deflected out of the He_N beam. In

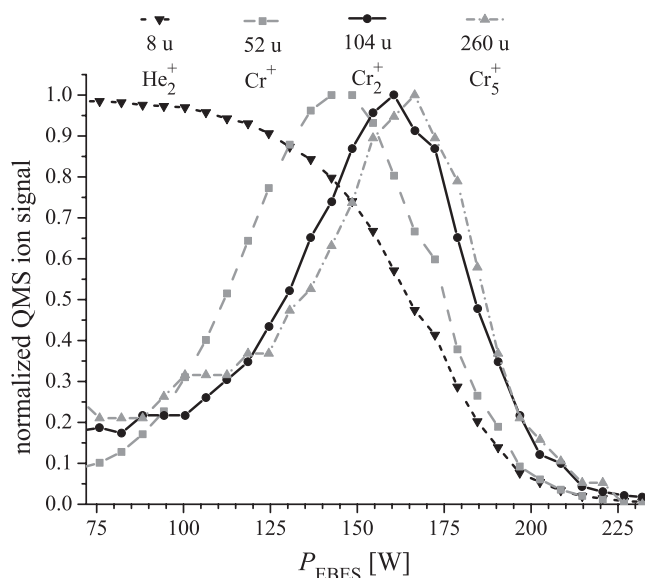


FIG. 3. Cr pickup statistics: dependency of the QMS ion signal of the masses 8 u (He_2^+), 52 u (Cr^+), 104 u (Cr_2^+), and 260 u (Cr_5^+) on the EBES heating power P_{EBES} . The droplet size distribution maximum is $\hat{N}_{50,15} = 5900$ He atoms per droplet. The signal of each mass is normalized individually.

the following, the droplet shrinkage due to both Cr pickup and cluster formation is estimated. The pickup process can be approximated by an inelastic collision at right angles,³⁷ which is governed by the velocities of the colliding partners. The Cr atoms are assumed to leave the EBES with velocities that follow a Maxwellian distribution. Their root-mean-square velocity is given by $v_{\text{Cr}} = \sqrt{3k_B T_{\text{EBES}}/m_{\text{Cr}}}$, where k_B is the Boltzmann constant, T_{EBES} is the EBES temperature, and $m_{\text{Cr}} = 52$ u is the atomic mass of Cr. With $T_{\text{EBES}} = (1600 \pm 50)^\circ\text{C}$ we obtain $v_{\text{Cr}} = (950 \pm 20)$ m/s. The He_N velocity is calculated from conservation of enthalpy,⁴¹ $v_{\text{He}_N} = \sqrt{2(h_0 - h_{\lambda p})}$, where h_0 and $h_{\lambda p}$ are the specific enthalpies at stagnation conditions and at the lambda point, respectively.⁴² For $p_0 = 50$ bar and $T_0 = 15$ K one obtains $v_{\text{He}} = 389$ m/s. Considering momentum conservation

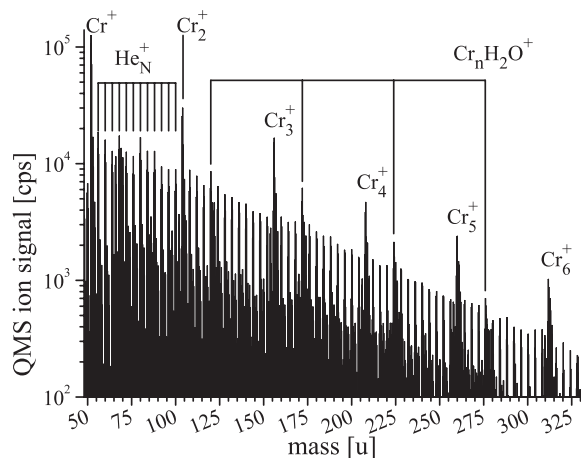


FIG. 4. Mass spectrum showing Cr_n^+ ($1 \leq n \leq 6$) ion yields. Additionally, the combination of Cr_n^+ with water and its fragments (H_2O , OH , O), and the typical He_N^+ fragments are visible. The spectrum is recorded with $\hat{N}_{50,15} = 5900$ He atoms per droplet and $P_{\text{EBES}} = 160$ W.

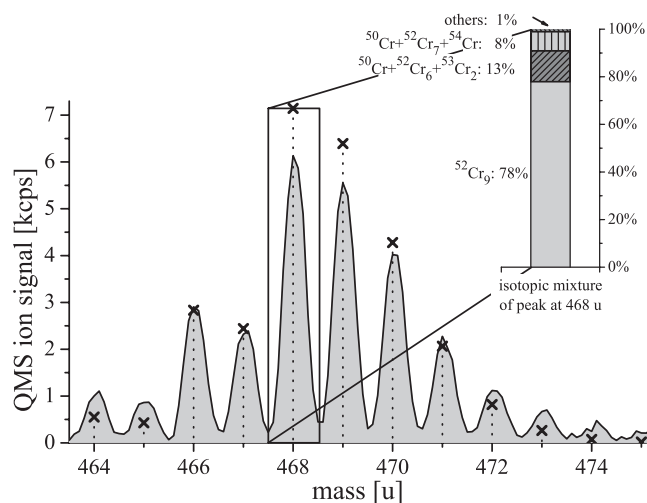


FIG. 5. Mass spectrum showing the most abundant part of the isotopic mixture of Cr_9^+ , as obtained with large He_N ($\hat{N}_{75,14} = 8700$). The simulated mass distribution according to the Cr isotopic abundances is indicated by crosses. The inset shows the simulated composition of the most prominent peak at 468 u.

of the inelastic scattering process at right angle, the difference in kinetic energy of the colliding partners before and after the inelastic collision gives the dissipated energy E_{dis} and thus the number of He atoms which are evaporated from the He_N . With the given parameters we estimate E_{dis} for the pickup of one Cr atom to be (281 ± 6) meV (corresponding to (3270 ± 80) K; $1 \text{ K} \triangleq 8.62 \times 10^{-5} \text{ eV} \triangleq 1.38 \times 10^{-23} \text{ J}$). The binding energy of He atoms to the droplet depends on the droplet size and we take an average value of 6.2 K ($\triangleq 0.53$ meV) per He atom.⁴³ Thus, the He_N are expected to shrink by 530 ± 20 He atoms for each Cr atom pickup.

Droplet shrinkage due to the formation of Cr_n inside He_N upon multiple Cr atom pickup is more difficult to estimate, because the type of bonding of Cr_n in He_N is unclear. Resonant two-photon ionization studies of Cr_2 find a singlet ground state⁴⁴ with a binding energy of (1.54 ± 0.06) eV.³ When a Cr_2 singlet state is formed inside a He_N 2900 ± 100 He atoms are evaporated. Adding the evaporated He atoms for the pickup of two Cr atoms this amounts to 3960 ± 140 for the pickup and formation of Cr_2 . However, since oligomers of alkali metals and silver were found in high spin configurations^{20–22} the bonding of Cr_2 in He_N remains to be determined. We note that the binding energy per Cr atom in the bulk is 4.1 eV (Ref. 45) so that for larger Cr_n clusters an increasingly higher value than 1.54 eV has to be taken. For small clusters produced in this work we take the number of 2900 ± 100 evaporated He atoms for the attachment of single Cr atoms as constant.

Figure 4 shows a QMS scan in the mass region of Cr^+ to Cr_6^+ . In addition to Cr_n^+ , a comb-like structure of equidistant peaks separated by 4 u appears in the spectrum. These peaks represent He_N fragment ions. The Cr_n^+ peaks stick out of this comb separated by 52 u, which is the mass of the most abundant Cr isotope. The peaks seem to be broadened at higher n , which can be explained by the different isotopic mixtures of Cr_n (this is shown in more detail in Fig. 5 for Cr_9^+). Ion signals in the range of 16 u to 18 u above each Cr_n^+ peak indicate

the existence of $\text{Cr}_n\text{H}_2\text{O}^+$ and their fragments (Cr_nOH^+ and Cr_nO^+). H_2O is present in the residual gas and thus accidentally picked up by the He_N .

The appearance of Cr_6 is reasonable considering the droplet size distribution with $\hat{N}_{50,15} = 5900$ in combination with the estimation of droplet shrinkage upon pickup and cluster formation given above. In this worst case approximation, the pickup of six Cr atoms plus five times the Cr_2 binding energy sums up to $17\,700 \pm 600$ He atoms, which are evaporated. According to the log-normal distribution $16\% \pm 2\%$ of the droplets are big enough to survive the pickup and formation of Cr_6 . However, we note that it is not possible to deduce the actual Cr_n flux rate from measured Cr_n^+ ion yields due to several reasons such as (1) droplet size dependent electron impact ionization of Cr_n - He_N complexes, (2) droplet size dependent ionization of Cr_n inside He_N , and (3) fragmentation of Cr_n upon ionization.

With the current setup the mass range of our QMS (1–500 u) limits the largest detectable Cr cluster to Cr_9 . In order to observe Cr_9 we used droplets of $\hat{N}_{75,14} = 8700$ atoms and $P_{\text{EBES}} = 180$ W. The most prominent region of the Cr_9^+ mass spectrum is shown in Fig. 5, together with the simulated mass distribution of different isotopic combinations (indicated by crosses). Each of the observed masses is a result of different isotopic combinations; the natural abundances are: ^{50}Cr : $\sim 4.3\%$, ^{52}Cr : $\sim 83.8\%$, ^{53}Cr : $\sim 9.5\%$, and ^{54}Cr : $\sim 2.4\%$. The simulated mass distribution and the composition of each peak is described by a multinomial distribution.⁴⁶ For example, the composition of the peak at 468 u is indicated in Fig. 5: $^{52}\text{Cr}_9$ (78%), $^{50}\text{Cr} + ^{52}\text{Cr}_6 + ^{53}\text{Cr}_2$ (13%), and $^{50}\text{Cr} + ^{52}\text{Cr}_7 + ^{54}\text{Cr}$ (8%), and the sum of all other combinations $\sim 1\%$. In the same manner as for Cr_6^+ in Fig. 4, the probability of the appearance of Cr_9^+ and the survival of corresponding droplets can be estimated. The pickup of nine Cr atoms plus eight times the Cr_2 binding energy results in the evaporation of $28\,000 \pm 1000$ He atoms. According to the log-normal distribution with $\hat{N}_{75,14} = 8700$ it can be estimated that $24\% \pm 2\%$ of the droplets survive this scenario.

IV. SUMMARY

In conclusion, we demonstrate a new source for stable and continuous doping of He_N with high-melting refractory metals. Heating is achieved by means of electron bombardment and temperatures of up to $(1650 \pm 50)^\circ\text{C}$ are reached. Several modifications to reach higher temperatures are discussed. The source is characterized by means of mass spectroscopic investigations of He_N doped with Cr atoms and clusters. The heating power of the Cr source and parameters of the He_N source are optimized for few and multiparticle pickup. The formation of Cr clusters with up to 9 Cr atoms in He_N is demonstrated and the probability of the appearance of Cr_9 is estimated for the given He_N size distribution.

ACKNOWLEDGMENTS

Discussions with Professor T. C. Steimle at the early stage of the source construction are gratefully acknowledged. Financial support is provided by the Austrian Science Fund

(FWF) under Grant No. P 22962 and the EFRE Program of the European Union and the Region of Styria.

- ¹W. A. de Heer and V. Kresin, in *Handbook of Nanophysics*, edited by K. Sattler (Taylor & Francis, London, 2010).
- ²J. Bansmann, S. H. Baker, C. Binns, J. A. Blackman, J. P. Bucher, J. Dorantes-Davila, V. Dupuis, L. Favre, D. Kechrakos, A. Kleibert, K. H. Meiwes-Broer, G. M. Pastor, A. Perez, O. Toulemonde, K. N. Trohidou, J. Tuailon, and Y. Xie, *Surf. Sci. Rep.* **56**, 189 (2005).
- ³B. Simard, M. A. Lebeault-Dorget, A. Marijnissen, and J. J. ter Meulen, *J. Chem. Phys.* **108**, 9668 (1998).
- ⁴B. O. Roos, A. C. Borin, and L. Gagliardi, *Angew. Chem., Int. Ed.* **46**, 1469 (2007).
- ⁵F. W. Payne, W. Jiang, and L. A. Bloomfield, *Phys. Rev. Lett.* **97**, 193401 (2006).
- ⁶M. J. Pellin, D. M. Gruen, T. Fisher, and T. Foosnaes, *J. Chem. Phys.* **79**, 5871 (1983).
- ⁷M. Vala, R. Pyzalski, J. Shakhsemampour, M. Eyring, J. Pyka, T. Tipton, and J. C. Rivoal, *J. Chem. Phys.* **86**, 5951 (1987).
- ⁸M. J. Pellin and D. M. Gruen, *J. Chem. Phys.* **79**, 5887 (1983).
- ⁹M. Moskovits, W. Limm, and T. Mejean, *J. Chem. Phys.* **82**, 4875 (1985).
- ¹⁰L. Fang, B. Davis, H. Y. Lu, and J. R. Lombardi, *J. Phys. Chem. A* **105**, 9375 (2001).
- ¹¹M. B. Knickelbein, *Phys. Rev. A* **67**, 013202 (2003).
- ¹²J. I. Martinez and J. A. Alonso, *Phys. Rev. B* **76**, 205409 (2007).
- ¹³P. Ruiz-Diaz, J. L. Ricardo-Chavez, J. Dorantes-Davila, and G. M. Pastor, *Phys. Rev. B* **81**, 224431 (2010).
- ¹⁴R. J. Vanzee, C. A. Baumann, and W. Weltner, *J. Chem. Phys.* **82**, 3912 (1985).
- ¹⁵C. Callegari and W. E. Ernst, in *Handbook of High Resolution Spectroscopy*, edited by F. Merkt and M. Quack (Wiley, Chichester, 2011).
- ¹⁶J. P. Toennies and A. F. Vilesov, *Angew. Chem., Int. Ed.* **43**, 2622 (2004).
- ¹⁷J. Tiggesbäumker and F. Stienkemeier, *Phys. Chem. Chem. Phys.* **9**, 4748 (2007).
- ¹⁸E. Loginov, L. F. Gomez, N. Chiang, A. Halder, N. Guggemos, V. V. Kresin, and A. F. Vilesov, *Phys. Rev. Lett.* **106**, 233401 (2011).
- ¹⁹E. Loginov, L. F. Gomez, and A. F. Vilesov, *J. Phys. Chem. A* **115**, 7199 (2011).
- ²⁰F. Stienkemeier, W. E. Ernst, J. Higgins, and G. Scoles, *J. Chem. Phys.* **102**, 615 (1995).
- ²¹M. Theisen, F. Lackner, and W. E. Ernst, *J. Phys. Chem. A* **115**, 7005 (2011).
- ²²A. Przysławski, P. Radcliffe, S. G. Gode, K. H. Meiwes-Broer, and J. Tiggesbäumker, *J. Phys. B: At., Mol. Opt. Phys.* **39**, S1183 (2006).
- ²³M. Koch, G. Auböck, C. Callegari, and W. E. Ernst, *Phys. Rev. Lett.* **103**, 035302 (2009).
- ²⁴M. Koch, C. Callegari, and W. E. Ernst, *Mol. Phys.* **108**, 1005 (2010).
- ²⁵J. Nagl, G. Auböck, C. Callegari, and W. E. Ernst, *Phys. Rev. Lett.* **98**, 075301 (2007).
- ²⁶G. Auböck, J. Nagl, C. Callegari, and W. E. Ernst, *J. Phys. Chem. A* **111**, 7404 (2007).
- ²⁷G. Auböck, J. Nagl, C. Callegari, and W. E. Ernst, *J. Chem. Phys.* **129**, 114501 (2008).
- ²⁸E. Loginov and M. Drabbels, *J. Phys. Chem. A* **111**, 7504 (2007).
- ²⁹K. J. Ross and B. Sonntag, *Rev. Sci. Instrum.* **66**, 4409 (1995).
- ³⁰M. Mudrich, B. Forkl, S. Müller, M. Dvorak, O. Bünermann, and F. Stienkemeier, *Rev. Sci. Instrum.* **78**, 103106 (2007).
- ³¹M. Koch, J. Lanzersdorfer, C. Callegari, J. S. Muentner, and W. E. Ernst, *J. Phys. Chem. A* **113**, 13347 (2009).
- ³²T. Steimle, D. Fletcher, K. Jung, and C. Scurlock, *Chem. Phys. Lett.* **184**, 379 (1991).
- ³³M. Lewerenz, B. Schilling, and J. P. Toennies, *Chem. Phys. Lett.* **206**, 381 (1993).
- ³⁴J. Harms, J. P. Toennies, and F. Dalfovo, *Phys. Rev. B* **58**, 3341 (1998).
- ³⁵E. L. Knuth, B. Schilling, and J. P. Toennies, *On Scaling Parameters for Predicting Cluster Sizes in Free Jets*, Rarefied Gas Dynamics Vol. 1, edited by J. Harvey and G. Lord, (Oxford University Press, Oxford, 1995), p. 270.
- ³⁶E. L. Knuth, *J. Chem. Phys.* **107**, 9125 (1997).
- ³⁷M. Lewerenz, B. Schilling, and J. P. Toennies, *J. Chem. Phys.* **102**, 8191 (1995).
- ³⁸G. Auböck, J. Nagl, C. Callegari, and W. E. Ernst, *Phys. Rev. Lett.* **101**, 035301 (2008).

- ³⁹A. Volk, J. Poms, M. Koch, and W. E. Ernst, *J. Phys. Chem. A* **115**, 7065 (2011).
- ⁴⁰A. M. Ellis and S. Yang, *Phys. Rev. A* **76**, 032714 (2007).
- ⁴¹H. Buchenau, E. L. Knuth, J. Northby, J. P. Toennies, and C. Winkler, *J. Chem. Phys.* **92**, 6875 (1990).
- ⁴²R. D. McCarty, *J. Phys. Chem. Ref. Data* **2**, 923 (1973).
- ⁴³S. A. Chin and E. Krotscheck, *Phys. Rev. B* **52**, 10405 (1995).
- ⁴⁴D. L. Michalopoulos, M. E. Geusic, S. G. Hansen, D. E. Powers, and R. E. Smalley, *J. Phys. Chem.* **86**, 3914 (1982).
- ⁴⁵D. Lide, *CRC Handbook of Chemistry and Physics* (CRC, Boca Raton, FL, 2006).
- ⁴⁶M. Evans, N. Hastings, and J. Peacock, *Statistical Distributions*, Wiley Series in Probability and Statistics (Wiley, New York, 2000).